NE-CAT Communications

A Biannual Newsletter of the Northeastern Collaborative Access Team Summer 2011

National Center for Research Resources

Message from the Director

Steve Ealick

Many developments have come to NE-CAT since the start of the year. We are preparing for remote access, simplifying the user interface, getting ready for the arrival of the PILATUS-6M and generally improving operation of the beamlines. We will also being getting an improved 25 Hz PILATUS-6M. This upgraded model (compared to the 12 Hz described in the previous newsletter) will be significantly faster. This is great news for our users as NE-CAT user productivity remains high. In 2010 and 2011, so far, we have the highest number of publications compared to any the other of APS macromolecular crystallography sectors.

We are still in limbo awaiting the decision by Congress on NCRR. The decision on closing NCRR should be made in July. Despite this uncertainty, we are moving forward with our P41 grant renewal. To this goal, we had a meeting with our Resource Advisory Committee on April 29 to discuss new core research areas and the science that will drive the technical and software developments for these cores at NE-CAT.

If you want to hear, not read, more about recent developments at NE-CAT, Frank Murphy will be giving a seminar at Harvard on June 22. I encourage all our users in the Boston area to attend. For further information on our beamline capabilities or to check out available beamtime, please visit our website at http://necat.chem.cornell.edu.

Beamline Developments

1. Axis Video Servers & Improved Visualization

The analog video feed from the in-line camera for the MD2 microdiffractometers is tapped and fed to a video encoder (also known as a video server) by Axis Communications. The Axis video server digitizes the video feed into MPEG format and sends it over the network to various computers. For example, the user interface on the auxiliary computer displays this video feed for crystal centering. This video feed is also used for automated beam alignment.

New Axis video servers were installed on both beamlines in March. These servers are faster, more powerful and provide more MPEG video options than the original servers. This allows a faster video feed with less lag, which will be beneficial when remote access is enabled at NE-CAT.

2. Remote Beamline Access

In preparation for remote access to the beamline, a Remote Access Channel (RAC) has been added to our core beamline software, CONSOLE. Through this RAC, CONSOLE can receive commands in the form of “button-clicks” and take appropriate actions. On the client side, an HTML5 web-based user interface (UI) is under development. Key clicks on this web-based UI are transferred to CONSOLE through a Python-based backend.

3. Ice Reduction in the Automounter Storage Dewars

Ice in the sample storage dewar is undesirable at any time. For this reason, at NE-CAT, the dewars are de-frosted and dried once a week when beam is unavailable due to Machine Studies. Ice formation in the storage dewars at NE-CAT is minimal, but attempts to reduce it further have resulted in a new design for the felt barrier at the interface between the metal dewar and the transparent monolithic lid.

When the dewar moves around under the lid, it is possible for condensation to build up on the underside of the lid. Fans pointed at the lid are used to evaporate the condensation and the old felt barrier also absorbed liquid. However, during humid weather, the possibility exists for the felt barrier to become saturated with liquid, cease to absorb and contribute to ice formation inside the dewar.

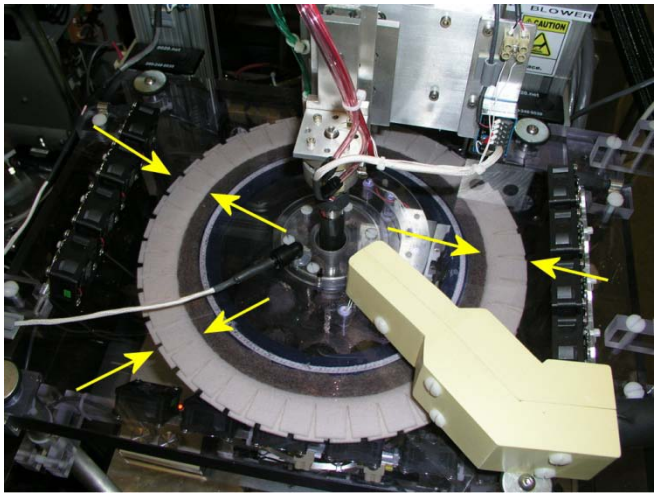

Fig. 1 The new felt barrier for the sample storage dewar. Yellow arrows show the location of the new ice barrier.

Therefore, at the end of April, a new felt barrier was added to the sample dewar to further reduce the production of ice. The new barrier is composed of two layers of felt cut at intervals to create a toothed skirt that can sweep across the underside of the lid to absorb moisture. The layers are offset so that the teeth of the skirt interleave to prevent air and moisture penetration.

4. Preparation for PILATUS-6M Installation

Delivery of the PILATUS-6M is expected in the latter half of the 2011 calendar year. With the PILATUS-6M, short, shutterless exposures can be expected to be the norm for data collection. This will require a very stable beam. Currently, residual beam motion is compensated by performing three sweeps through the desired oscillation angle during a single exposure. With shutterless operation, multi-sweep exposures cannot be used to compensate for residual beam motion.

In order to take advantage of the PILATUS-6M's shutterless operation mode, NE-CAT must eliminate as many sources of potential beam instability as possible. Beam stability can be compromised by monochromator vibration caused by liquid nitrogen (LN_2) flow for cooling and floor vibrations. In preparation for arrival of the PILATUS-6M, tests were performed in January/February to determine the effect of vibration on beam stability caused by the LN_2 flow rate and from floor vibrations.

These tests showed that floor vibrations and turbulence from delivery of LN_2 were being transferred to the monochromator. Some floor vibrations could be dampened by stabilizing to the monochromator housing with lead weights. A more extensive modification of the monochromater is needed to eliminate vibration caused by LN_2 delivery.

The PILATUS-6M will be installed on the C line which has a Kohzu dual crystal monochromator. Two potential sources of vibration or motion transfer within the monochromator are the standoffs holding each crystal and the hoses that deliver the LN_2. Modifications to the monochromator were made during the May shutdown to reduce vibration by these sources.

Each crystal is supported by four individual standoffs. These standoffs could move independently of each other during operation and can torque the crystal in up to 4 different directions as a result of vibrations from LN_2 flow. During the May shutdown, the individual standoffs for each crystal were replaced with a single, solid block. It is believed that the solid block will provide more stability for the crystal than the individual standoffs and be less likely to asynchronously transfer LN_2 flow vibrations. Preliminary tests and observations show a considerable improvement in beam stability.

The metal hoses delivering LN_2 to the crystals are corrugated. When LN_2 flows over the corrugation, turbulence from the liquid can cause vibration. A smoother inner bore would lessen the turbulence. The corrugated metal hoses inside the monochromater will be remodeled during the upcoming Fall shutdown. This allows testing of the sold block supports to determine their effectiveness in eliminating vibrations prior to installation of modified metal hoses.

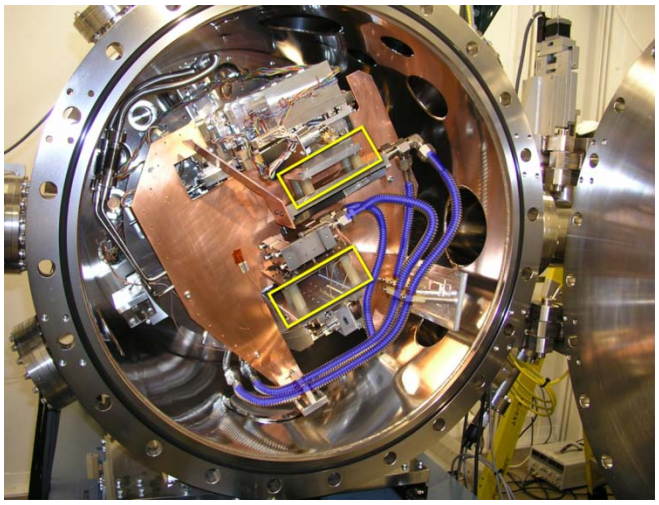

Fig. 2 This shows the interior of the dual crystal monochromator on the C line. The standoffs supporting each crystal have been outlined in yellow. The hoses delivering LN_2 have been highlighted in blue.

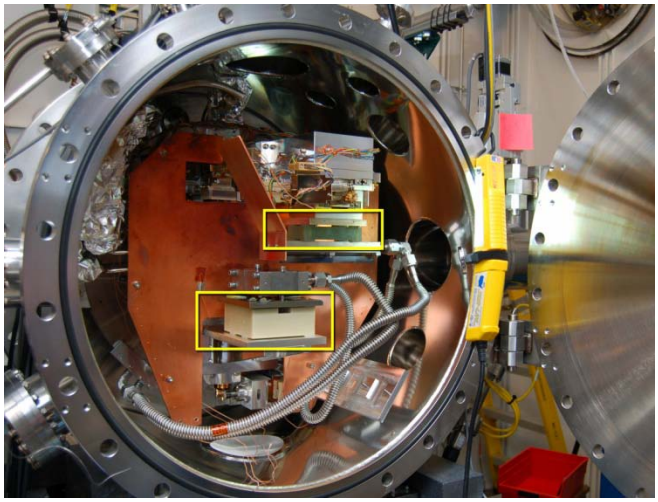

Fig. 3 This shows the interior of the dual crystal monochromator on the C line after the standoffs have been replaced with solid blocks. The blocks have been outlined in yellow.

5. RAPD

RAPD, our online data analysis suite, has also received many new improvements. Among the additions are: improved data set analysis, data set merging, data set re-integration, and a new molecular replacement (MR) pipeline.

The improved data set analysis includes a query of the PDB for similar crystals and a quick MR for suitable candidates. In addition, the data set is tested for pseudo-translation and twinning via XTRIAGE and the presence of non-crystallographic symmetry can be determined from self-rotation plots via MOLREP. These actions occur automatically for every dataset.

The MR pipeline allows the user to submit a pre-chosen PDB file or code. Molecular replacement is then performed using PHASER. All the possible space groups are tested simultaneously and if a correct solution is found, the user has the option to download the reflection file with the phases as well as the model.

Due to the combination of radiation damage and the small size of crystals that frequent NE-CAT beamlines, merging multiple data sets is often required to build a complete data set. The new merging protocol (SimpleMerge) allows users to take two different integrated datasets and merge them together. SimpleMerge assigns a reference data set and base space group using POINTLESS. It then determines the highest possible resolution and rescales while checking that the datasets to be merged are indexed identically. The user can check the quality of this merged data using the same analysis as that for single data sets.

With access to the computer cluster, RAPD can quickly integrate datasets during collection. This real time integration allows the user to evaluate data as it is collected. However, due to bad frames from crystal defects (such as cracks or multiple lattices) or beam loss, the initial integration can truncate prior to the end of a run, fail to integrate in the correct point group or fail to scale in the correct space group. Therefore, re-integration has been made available which allows the user to eliminate bad frames by indicating different starting and ending frames. The user can ask for re-integration via RAPD or XIA2. RAPD is faster than XIA2, but the XIA2 suite makes an exhaustive effort to optimize data integration and scaling.

6. Workshop

NE-CAT will be hosting a workshop on “Advances in Low to Moderate Resolution Phasing and Refinement” at Rockefeller University on September 19, 2011. New York City was chosen as the location for the workshop because of its proximity to the NE-CAT member institutions. The workshop is organized by NE-CAT (Kay Perry, Igor Kourinov and Raj Rajashankar) in cooperation with Rockefeller University (Seth Darst).

This is a one day workshop covering low resolution phasing and refinement, use of EM structures to phase X-ray data, SAXS, hardware for low resolution data collection, and use of molecular replacement in phasing low resolution data. Axel Brunger, Malcolm Capel, Steve Harrison, Randy Read, John Tainer, Tom Terwilliger, Yong Xiong, Frank Dimaio from the lab of David Baker and Silvia Russi from the lab of Florent Cipriani have all agreed to speak at the workshop. More information can be found at the NE-CAT website (http://necat.chem.cornell.edu/workshops/lowresolutionworkshop.php).

The workshop is free. However, the lecture hall space at Rockefeller limits us to 75 participants. There has been huge interest in this workshop and registration is already closed. For those who cannot attend, we have plans for posting a video of the proceedings on the website.

Research Highlights

Structure of IκB kinase β (IKKβ)

Hao Wu, Weill Cornell Medical College, Department of Biochemistry, New York, NY

IκB kinase (IKK) is required for the activation of NF-κB by phosphorylating its inhibitor protein IκB, leading to its proteasomal degradation. This then allows NF-κB to enter the nucleus for target gene transcription. IKK is a large protein complex containing the kinase subunit IKKα and/or IKKβ, and the regulatory protein NEMO (IKKγ). IKKβ contains an N-terminal kinase domain, a ubiquitin-like domain (ULD) domain, predicted leucine zipper (LZ) and helix-loop-helix (HLH) domains and a C-terminal NEMO-binding domain (NBD). It plays a dominant role in the canonical NF-κB pathway by phosphorylating IκBα. IKKα shares more than 50% sequence identity with IKKβ and plays an indispensible role in the non-canonical NF-κB pathway.

Because of the central importance of IKKβ in NF-κB biology and its potential as a therapeutic target against cancer and inflammation, the structure of IKKβ has been heavily pursued by both academia and industry. My postdoctoral fellow Guozhou Xu (Fig. 5) was able to crystallize an almost full-length IKKβ lacking only the C-terminal NBD for which the structure is already known. The initial crystals are in the P1 space group with eight molecules in the crystallographic asymmetric unit, a total molecular mass of ~1.3 MDa. We encountered many difficulties in solving the phases of the crystal form, sometimes because of the large number of heavy atom sites such as in the case of Se, Hg and Au derivatives, and other times because of weak derivative signals as in the case of an Yb derivative. Eventually, we crystallized IKKβ in an alternative crystal form that belongs to the $I4_122$ space group with one molecule per asymmetric unit. We solved this structure from a Se-MAD data set at 4.0 Å resolution. We then solved the P1 structure using molecular replacement and refined it to 3.6 Å resolution. All crystal screening and data collection were performed at NE-CAT, taking advantage of the bright beamlines.

One surprising finding is that the LZ and HLH domains were falsely predicted; instead, this region of the structure forms an elongated helical bundle we dubbed the scaffold/dimerization domain (SDD). IKKβ exists as dimers in solution and together with biochemical and

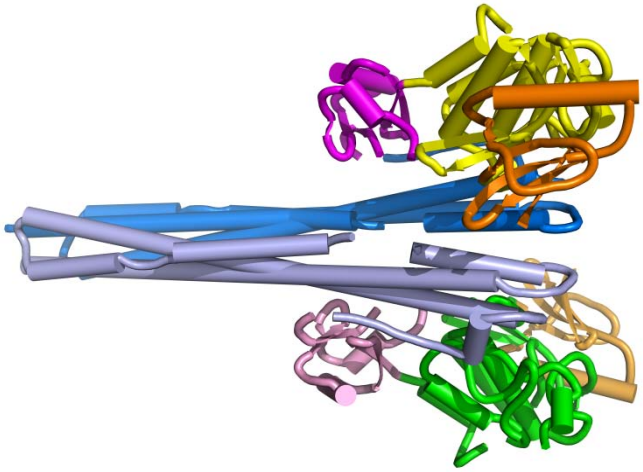

Fig. 4 Crystal structure of IKKβ dimer. KD: orange, yellow, green and gold; ULD: magenta and pink; SDD: blue and light blue.

mutagenesis studies, we showed that dimerization is mediated by the SDD domain. The IKKβ dimer structure has the shape of a pair of shears with the KD and the ULD forming the "handle" and the SDD being the "blade" (Fig. 4). The three domains intimately interact with each other, which makes IKKβ an integral trimodular unit. Our functional assays further elucidated that the ULD and SDD mediates a critical interaction with IκBα to restrict substrate specificity, and the ULD is required for catalytic activity. Interestingly, dimerization is no longer necessary to maintain the kinase activity once IKKβ is activated. However, dimerization of IKKβ is required for its activation upon overexpression. In both the P1 and the $I4_122$ space groups, IKKβ molecules further dimerize into conserved tetramers with 222 symmetry. In the tetramers, the KDs of neighboring IKKβ molecules face each other and may mediate auto-trans-phosphorylation and activation. This work was recently published in Nature (Xu, G. et. al, Nature, 2011 Apr 21; 472(7343): 325-30.)

Fig. 5 Guozhou Xu, who performed the primary work on IKKβ, at his graduation ceremony prior to joining Hao Wu's lab.

The high-quality beamlines at NE-CAT played a key role in the structure determination of IKKβ. Since all IKKβ crystals diffract weakly and only to medium resolutions, the bright and versatile beamlines were especially critical for collecting adequate and accurate data for phase determination. The outstanding technical support of NE-CAT, especially from Dr. N. Sukumar and Dr. K. Rajashankar, was indispensable in the success of the data collection and structure determination.

Metal ion export in bacteria

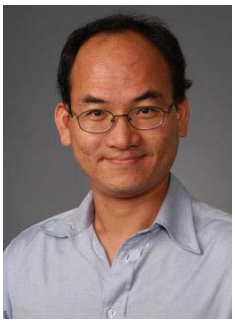

Edward W. Yu, Department of Chemistry, and Department of Physics and Astronomy, Iowa State University, Ames, IA 50011, USA

In Gram-negative bacteria, efflux systems of the resistance-nodulation-division (RND) family play major roles in the intrinsic and acquired tolerance of antibiotics and toxic compounds (Tseng et al., 1999). They represent key components for Gram-negative pathogens to use in overcoming toxic environments unfavorable for their survival. An RND efflux pump (or transporter) works in conjunction with a periplasmic membrane fusion protein (or adaptor), and an outer membrane channel to form a functional protein complex. In *Escherichia coli*, one such tripartite efflux system CusCBA is responsible for extruding biocidal Cu(I)/Ag(I) ions (Franke et al. 2003). CusA is a large RND efflux pump that depends on the proton-motive-force. It assembles with the CusB membrane fusion protein and CusC outer membrane channel to export these metal ions out of the cell.

To elucidate the mechanisms used by the CusCBA system for Cu(I)/Ag(I) recognition and extrusion, we determined the crystal structure of the full-length CusB membrane fusion protein at a resolution of 3.40 Å, revealing four linearly-arranged domains (Su et al., 2009). Overall, CusB is folded into an elongated structure, ~120 Å long and ~40 Å wide. The first three domains (Domains 1-3) of the protein are mostly β-strands. However, the fourth domain (Domain 4) is all α-helices and is folded into a three-helix bundle structure (Fig. 6a).

We also determined the crystal structure of the full-length CusA RND pump at 3.52-Å resolution (Long et al., 2010). The structure suggests that CusA exists as a homotrimer (Fig. 6b). Each subunit of CusA consists of 12 transmembrane helices (TM1-TM12) and a large periplasmic domain formed by two periplasmic loops between TM1 and TM2, and TM7 and TM8, respectively. The periplasmic domain of CusA can be divided into a pore domain (comprising sub-domains PN1, PN2, PC1, PC2) and a CusC docking domain (containing sub-domains DN and DC). In addition, PC1 and PC2 form an external cleft facing the periplasm, and this cleft is closed in the apo-CusA structure.

A most interesting feature appears in the cleft of the periplasmic domain with residues located on the left side of the wall tilting into the cleft to close the opening. Residues 665-675, located at the bottom of the cleft, form a horizontal α-helix. Three proximal methionines, M573, M623 and M672, creating a three-methionine specific binding site, are found above this helix.

The bound Cu(I)/Ag(I) is found to coordinate residues M573, M623 and M672. Binding of Cu(I)/Ag(I) initiates significant conformational changes in the periplasmic as well as transmembrane domains of CusA. The most noticeable difference between the apo and ion-bound structures appears in the PC2 region (Fig. 6c). A shift in position of the entire PC2 sub-domain is found in the ion-bound form. This shift results in formation of the cleft between sub-domains PC1 and PC2. The shift can be interpreted as a 30^{o} swing of PC2. The horizontal helix located inside the cleft also makes a substantial movement. The C-terminal end of this helix is found to tilt upward by 21^{o} in the ion-bound form in comparison with the apo structure (Fig. 6d). This tilting motion allows M672 to move closer to M573 and M623, forming a transient three-sulfur coordination site. Coupled with this movement, TM8 also shifts in position to a more vertical orientation. Overall, the N-terminal end of TM8 is found to shift away from the core by 10 Å after metal binding.

In addition, the structures indicate that each protomer of CusA forms a channel spanning the entire transmembrane region up to the bottom of the periplasmic funnel. Intriguingly, this channel includes four methionine-pairs (M410-M501, M403-M486, M391-M1009, and M271-M755) as well as the three-methionine binding site (M573, M623 and M672). Genetic analysis and transport assays suggest that CusA utilizes these methionines to bind and export metal ions. These structures suggest a stepwise shuttle mechanism for transport between these sites.

To examine how CusA and CusB assemble as a functional unit, we co-crystallized the CusBA adaptor-transporter efflux complex. The co-crystal structure (at 2.90-Å resolution) revealed that each protomer of CusA interacts specifically with two elongated molecules of CusB (molecules 1 and 2) at the upper half portion of the periplasmic domain (Su et al., 2011). The two CusB adaptors are tilted at an angle of ~50^{o}

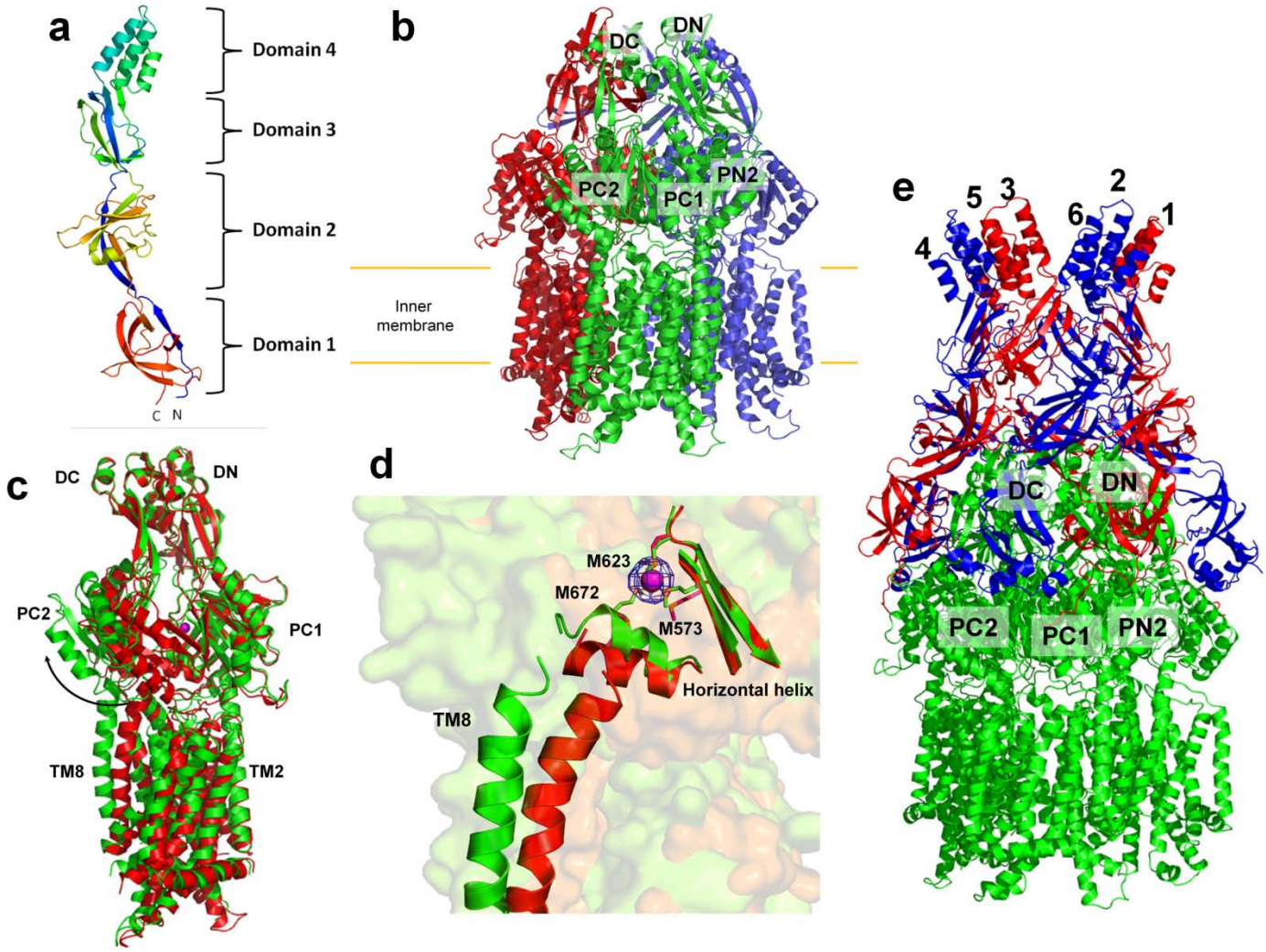

Fig. 6 (a) Structure of the CusB membrane fusion protein. (b) Structure of the CusA inner membrane efflux pump. (c) Superimposition of apo-CusA (red) onto CusA-Cu(I) (green). The bound Cu(I) is in pink. Arrow indicates the shift of PC2 when comparing these two structures. (d) Anomalous map of the bound Cu(I), contoured at 8σ, is in blue. The bound Cu(I) is shown as a pink sphere. M573, M623 and M672 are shown as sticks. The changes in conformation of the horizontal helix and TM8, are shown in a superimposition of the structures of apo (red) and Cu(I)-bound (green) CusA. (e) Structure of the CusBA heavy-metal efflux complex.

with respect to the membrane surface, and establish a close fit with the transporter at the concave surface formed by Domains 1 and 2 of the adaptor. Molecule 1 of CusB contacts mainly the upper regions of PN2 and PC1, and the DN sub-domain of CusA. Molecule 2 of CusB, however, predominantly bridges to the upper regions of PC1 and PC2, and also the sub-domain DC of the pump. These two adaptor molecules are also seen to specifically contact one another, primarily through Domains 1, 2 and 3 of these two elongated molecules. The trimeric CusA pump therefore directly contacts six CusB molecules, which form a channel at the top of the CusA trimer (Fig. 6e).

The hexameric arrangement of CusB creates a funnel-like structure. These protomers utilize a side-by-side packing arrangement to form this funnel. Domain 1 and the lower half of Domain 2 of CusB primarily create a cap-like structure whereas the upper half of Domain 2, and Domains 3 and 4 contribute to the central channel of the funnel. The inner surface of the cap fits closely with the outer surface of the upper portion of the CusA trimer. The channel formed above the cap of the adaptor is ~62 Å long with an average internal diameter of ~37 Å. Thus, the interior of the channel gives rise to a large elongated cavity with a volume of ~65,000 $Å^3$. Given the fact that six CusB molecules assemble to form a channel at the CusA funnel top, this suggests that the adaptor is likely to be involved in the active extrusion of metal ions.

Finally, we predicted a three-dimensional structure of the trimeric CusC outer membrane channel, and develop a model of the tripartite efflux assemblage.

This $CusC_3$-$CusB_6$-$CusA_3$ model presents a 750 kDa efflux complex spanning the entire bacterial cell envelope to export Cu(I)/Ag(I) ions.

References

Tseng, T. T., Gratwick, K. S., Kollman, J., Park, D., Nies, D. H., Goffeau, A., and Saier, M. H. Jr. (1999). The RND permease superfamily: an ancient, ubiquitous and diverse family that includes human disease and development protein. *J. Mol. Microbiol. Biotechnol. 1,* 107-125.

Franke, S., Grass, G., Rensing, C., and Nies, D. H. (2003). Molecular analysis of the copper-transporting efflux system CusCFBA of *Escherichia coli*. *J. Bacteriol. 185,* 3804-3812.

Su, C.-C., Yang, F., Long, F., Reyon, D., Routh, M. D., Kuo, D. W., Mokhtari, A. K., Van Ornam, J. D., Rabe, K. L., Hoy, J. A., Lee, Y. J., Rajashankar, K. R., and Yu, E. W. (2009). Crystal structure of the membrane fusion protein CusB from *Escherichia coli*. *J. Mol. Biol. 393,* 342-355.

Long, F., Su, C.-C., Zimmermann, M. T., Boyken, S. E., Rajashankar, K. R., Jernigan, R. L., and Yu, E. W. (2010). Crystal structures of the CusA efflux pump suggest methionine-mediated metal transport mechanism. *Nature 467, 484-488.*

Su, C.-C., Long, F., Zimmermann, M. T., Rajashankar, K. R., Jernigan, R. L., and Yu, E. W. (2010). Crystal structure of the CusBA heavy-metal efflux complex of *Escherichia coli*. *Nature 470,* 558-562.

Staff Activities

Talks

Kanagalaghatta Rajashankar, "Microdiffraction: What can be done?" INDO-US Workshop/Symposium on Modern Trends in Macromolecular Structures, Indian Institute of Technology Bombai, Mumbai-400076, India, February 21-24, 2011.

Kanagalaghatta Rajashankar, "Workshop on Macromolecular Structure Determination (Advanced Level)" INDO-US Workshop/Symposium on Modern Trends in Macromolecular Structures, Indian Institute of Technology Bombai, Mumbai-400076, India, February 21-24, 2011.

Malcolm Capel and Frank Murphy, "Vector Scanned Microcrystallographic Data Collection Techniques," 2011 Annual Meeting of the American Crystallographic Association, New Orleans, Louisiana, May 28 – June 2, 2011.

Narayanasami Sukumar, "Defining the role of the axial ligand of the type 1 copper site in amicyanin, an electron transfer protein from Paracoccus denitrificans," 2011 Annual Meeting of the American Crystallographic Association, New Orleans, Louisiana, May 28 – June 2, 2011

Posters

Surajit Banerjee, Kelsey C. Duggan, Daniel J. Hermanson, Joel Muse, Jeffery J. Prusakiewicz, Jami L. Scheib, Bruce D. Carter, John A. Oates, Lawrence J. Marnett, "Structural Insights into the Binding Mechanism of (R)- and (S)-Naproxen with Cyclooxygenase-2," 2011 Annual Meeting of the American Crystallographic Association, New Orleans, Louisiana, May 28 – June 2, 2011.

Kanagalaghatta Rajashankar , Steven Ealick, Malcolm Capel, Surajit Banerjee, Amit Belani, Anthony Lynch, Frank Murphy, Igor Kourinov, David Neau, Kay Perry, Cynthia Salbego, Jonathan Schuermann, Narayanasami Sukumar, James Withrow, "North Eastern CAT Crystallography Beam Lines for Challenging Structural Biology Research," 2011 Annual Meeting of the American Crystallographic Association, New Orleans, Louisiana, May 28 – June 2, 2011.

Publications

French, J. B., Neau, D. B., and Ealick, S. E. (2011) Characterization of the Structure and Function of Klebsiella pneumoniae Allantoin Racemase, J. Mol. Biol. (in press)

Peng, G., Sun, D., Rajashankar, K. R., Qian, Z., Holmes, K. V., and Li, F. (2011) Crystal structure of mouse coronavirus receptor-binding domain complexed with its murine receptor, Proc. Natl. Acad. Sci. U. S. A. (in press).

Larson, M. R., Rajashankar, K. R., Crowley, P. J., Kelly, C., Mitchell, T. J., Brady, L. J., and Deivanayagam, C. (2011) Crystal structure of the C-terminus of *Streptococcus mutans* antigen I/II and characterization of salivary agglutinin adherence domains, *J. Biol. Chem. 286*, 21657-21666.

Ding, F., Lu, C., Zhao, W., Rajashankar, K. R., Anderson, D. L., Jardine, P. J., Grimes, S., and Ke, A. (2011) Structure and assembly of the essential RNA ring component of a viral DNA packaging motor, *Proc. Natl. Acad. Sci. U. S. A. 108*, 7357-7362.

Cao, Y., Jin, X., Levin, E. J., Huang, H., Zong, Y., Quick, M., Weng, J., Pan, Y., Love, J., Punta, M., Rost, B., Hendrickson, W. A., Javitch, J. A., Rajashankar, K. R., and Zhou, M. (2011) Crystal structure of a phosphorylation-coupled saccharide transporter, *Nature 473*, 50-54.

Cao, Y., Jin, X., Huang, H., Derebe, M. G., Levin, E. J., Kabaleeswaran, V., Pan, Y., Punta, M., Love, J., Weng, J., Quick, M., Ye, S., Kloss, B., Bruni, R., Martinez-Hackert, E., Hendrickson, W. A., Rost, B., Javitch, J. A., Rajashankar, K. R., Jiang, Y., and Zhou, M. (2011) Crystal structure of a potassium ion transporter, TrkH, *Nature 471*, 336-340.

Su, C.-C., Long, F., Zimmermann, M. T., Rajashankar, K. R., Jernigan, R. L., and Yu, E. W. (2011) Crystal structure of the CusBA heavy-metal efflux complex of *Escherichia coli, Nature 470*, 558-562.

Lombardi, P. M., Angell, H. D., Whittington, D. A., Flynn, E. F., Rajashankar, K. R., and Christianson, D. W. (2011) Structure of Prokaryotic Polyamine Deacetylase Reveals Evolutionary Functional Relationships with Eukaryotic Histone Deacetylases, *Biochemistry 50*, 1808-1817.

Gilbert, N. C., Bartlett, S. G., Waight, M. T., Neau, D. B., Boeglin, W. E., Brash, A. R., and Newcomer, M. E. (2011) The structure of human 5-lipoxygenase, *Science 331*, 217-219.

Choi, M., Sukumar, N., Mathews, F. S., Liu, A., and Davidson, V. L. (2011) Proline 96 of the Copper Ligand Loop of Amicyanin Regulates Electron Transfer from Methylamine Dehydrogenase by Positioning Other Residues at the Protein-Protein Interface, *Biochemistry 50*, 1265-1273.

Committee Meetings

Malcolm Capel, BioCAT Resource Advisory Committee, June 7, 2011.

Acknowledgements

NE-CAT is supported by Grant (RR-15301) from the NIH National Center for Research Resources and contributions from the following NE-CAT institutional members:

Columbia University
Cornell University
Harvard University
Massachusetts Institute of Technology
Memorial Sloan-Kettering Cancer Center
Rockefeller University
Yale University